108. Synthesis and Solvent Effects on the Conformation of Hymenistatin 1

by **Robert K. Konat**[a]), **Dale F. Mierke**[a]), **Horst Kessler**[a])*, **Bernhard Kutscher**[b]), **Michael Bernd**[b]), and **Rainer Voegeli**[b])

[a]) Organisch-chemisches Institut, Technische Universität München, Lichtenbergstrasse 4, D–8046 Garching
[b]) *ASTA Medica AG*, Weissmüllerstrasse 45, D–6000 Frankfurt/Main

(29.III.93)

The cyclic octapeptide cyclo(-Pro-Pro-Tyr-Val-Pro-Leu-Ile-Ile-) (**1**), isolated from the *Hymeniacidon* sponge, was synthesized and examined conformationally using NMR and molecular-dynamics simulations. Most structural parameters of synthetic **1** are in accord with those reported for the isolated material. Our study indicates some small but significant differences in the assignment of the ^{1}H- and ^{13}C-NMR resonances from those of the natural material. The conformation was determined in both $CHCl_3$ and DMSO using ^{1}H-NMR and molecular-dynamics simulations. Both NOE's and coupling constants were used as experimental restraints during the simulations which utilized explicitly the same solvent as in the NMR study. The differences in the interaction of the solvent with **1** were examined, providing insight into the observed differences in conformation. The dominant conformation contains a βVIa turn about Ile^8-Tyr^3 including a Pro^1-Pro^2 *cis*-peptide bond and a βI or βII turn about Val^4-Ile^7 in $CHCl_3$ and DMSO, respectively.

1. Introduction. – Marine plants and animals have provided a large number of natural products with a variety of biological activities. Examples include calyculin [1], cyclotheonamides [2], cystodytes [3], and phenazine alkaloids [4]. In 1990, *Pettit* and coworkers described the isolation of a cyclic octapeptide **1** from the *Hymeniacidon* sponge collected in the Pacific Ocean [5]. The substance was of great interest because of the cytostatic activity found in the P388-test on murine lymphoblastic leukaemia (ED_{50} = 3.5 μg/ml). The structure of **1** was determined to be cyclo(-Pro-Pro-Tyr-Val-Pro-Leu-Ile-Ile-), and subsequently, **1** was named hymenistatin 1. Although thorough structural characterization of the material was reported, the synthesis of **1** was not carried out. We now describe the synthesis of **1** and compare its structural parameters and cytostatic activity with those reported for the natural material. In addition, the conformation of **1** is examined by NMR spectroscopy and molecular-dynamics (MD) simulations, employing distance and coupling-constant restraints, in both DMSO and $CHCl_3$. The MD simulations, carried out using the same solvent as the NMR studies, show small but significant differences which can be explained by the interaction between the solvent and peptide.

$$\overset{1}{\text{cyclo(-Pro}}\text{-}\overset{2}{\text{Pro}}\text{-}\overset{3}{\text{Tyr}}\text{-}\overset{4}{\text{Val}}\text{-}\overset{5}{\text{Pro}}\text{-}\overset{6}{\text{Leu}}\text{-}\overset{7}{\text{Ile}}\text{-}\overset{8}{\text{Ile}}\text{-)}$$

1

2. Results and Discussion. – 2.1. *Synthesis.* The linear peptide corresponding to **1** was synthesized using the Boc strategy and standard solid-phase techniques [6]. The peptide was cyclized to **1** between the Pro^2 carbonyl group and the Tyr^3 N-atom using the azide method [7]. The cyclic peptide **1** was purified by flash-chromatography, gel filtration, and reversed-phase HPLC. An alternative synthesis was carried out, where the linear peptide

was cyclized between the Leu[6] carbonyl group and the Ile[7] N-atom by *N*-[3-(dimethylamino)propyl]-*N'*-ethylcarbodiimide/1*H*-benzotriazol-1-ol (EDCI/BtOH). The peptide was characterized by NMR and FAB mass spectroscopy. A comparison of the analytical data of synthetic **1** with those reported for the natural product is given in *Table 1*. All

Table 1. *Analytical Data for Synthetic and Natural Hymenistatin 1* (**1**)

	Synthetic **1**[a])	Natural **1**[b])
FAB-MS (NBA)	*m/z* 894	*m/z* 893.5505
IR (KBr)	3308 (br.), 2967, 2936, 1649 (br.), 1621, 1516 cm^{-1}	3320, 2960, 2920, 1680, 1617, 1517 cm^{-1}
NMR ($CHCl_3$)	see *Table 2*	see *Table 2*
M.p.	186°	180–182°
$[\alpha]_D$	−145 (c = 1, $CHCl_3$)	−8.6 (c = 1, $CHCl_3$)

[a]) This work. [b]) Material isolated by *Pettit* and coworkers [5].

spectroscopic data of the material isolated from *Hymeniacidon* sponge were reproduced, with the exception of the specific rotation. This may arise from impurities in the isolated natural material. In spite of this, we can confirm that hymenistatin 1 is indeed cyclo(-Pro-Pro-Tyr-Val-Pro-Leu-Ile-Ile-) (**1**). Even the presence of a small set of additional signals in the ^{1}H-NMR spectrum, caused by another conformation in slow equilibrium with the major conformation (see below), are found in both the natural and synthetic materials. As ^{1}H- and ^{13}C-NMR chemical shifts are very sensitive to structural changes, it is highly unprobable that these spectra are similar when constitution, configuration, and conformation are not identical.

2.2. *NMR Studies.* 2.2.1. *Signal Assignment.* All ^{1}H- and ^{13}C-NMR resonances of hymenistatin 1 (**1**) in both $CHCl_3$ and DMSO were unambiguously assigned. The values obtained in $CHCl_3$ along with those reported for the isolated material (in $CHCl_3$) are given in *Table 2*. By comparing the ^{1}H-NMR spectra of natural and synthetic **1**, we could

Table 2. *^{1}H- and ^{13}C-NMR Chemical Shifts of Hymenistatin 1* (**1**) *in $CDCl_3$ at 300 K*[a])

Residue	Group	Synthetic **1**[b])		Natural **1**[c])	
		δ(^{1}H) [ppm]	δ(^{13}C) [ppm]	δ(^{1}H) [ppm]	δ(^{13}C) [ppm]
Pro[1]	CO	–	171.79	–	–
	H–C(α)	**4.08**	59.47	*4.20*	60.89
	$H_{pro\text{-}S}$–C(β)	2.16	**28.80**	2.15	*31.87*
	$H_{pro\text{-}R}$–C(β)	**1.77**		*1.93*	
	H–C(γ)	2.12	25.35	2.11	25.06
	H'–C(γ)	1.93		1.95	
	$H_{pro\text{-}S}$–C(δ)	3.70	47.56	3.72	47.35
	$H_{pro\text{-}R}$–C(δ)	3.35		3.38	
Pro[2]	CO		170.41		–
	H–C(α)	**4.16**	61.20	*4.10*	59.19
	$H_{pro\text{-}S}$–C(β)	2.14	**32.13**	2.16	*28.52*
	$H_{pro\text{-}R}$–C(β)	**1.92**		*1.77*	
	H–C(γ)	1.59	21.48	1.60	21.11
	H'–C(γ)	0.81		0.85	
	$H_{pro\text{-}R}$–C(δ)	3.25	47.21	3.29	46.94
	$H_{pro\text{-}S}$–C(δ)	3.19		3.21	

Table 2 (cont.)

Residue	Group	Synthetic **1**[b])		Natural **1**[c])	
		$\delta(^1H)$ [ppm]	$\delta(^{13}C)$ [ppm]	$\delta(^1H)$ [ppm]	$\delta(^{13}C)$ [ppm]
Tyr[3]	NH	7.26		–	
	CO		172.33		–
	H–C(α)	4.21	58.39	4.22	58.13
	$H_{pro\text{-}S}$–C(β)	3.29	36.97	3.29	36.67
	$H_{pro\text{-}R}$–C(β)	2.88		2.90	
	H–C(1′)		127.48		127.00
	H–C(2′),H–C(6′)	7.04	129.99	7.03	129.67
	H–C(3′),H–C(5′)	6.86	116.25	6.84	115.94
	H–C(4′)		156.73		156.56
	OH			8.70	
Val[4]	NH	7.56		7.58	
	CO		173.35		–
	H–C(α)	4.58	56.59	4.56	56.29
	H–C(β)	1.95	31.97	1.95	31.67
	Me(γ)	0.98	19.61	0.98	19.29
	Me(γ′)	0.98	18.47	0.98	18.19
Pro[5]	CO		171.85		–
	H–C(α)	3.78	63.45	3.79	63.11
	$H_{pro\text{-}S}$–C(β)	2.29	30.28	2.31	30.00
	$H_{pro\text{-}R}$–C(β)	1.93		1.91	
	H–C(γ)	2.07	25.07	2.08	24.75
	H′–C(γ)	2.04		2.06	
	$H_{pro\text{-}R}$–C(δ)	3.91	48.87	3.92	48.55
	$H_{pro\text{-}S}$–C(δ)	3.66		3.68	
Leu[6]	NH	6.22		6.25	
	CO		172.22		–
	H–C(α)	4.00	55.97	3.98	55.79
	$H_{pro\text{-}R}$–C(β)	1.97	39.55	1.96	39.27
	$H_{pro\text{-}S}$–C(β)	1.81		1.82	
	H–C(γ)	1.52	25.63	1.55	25.31
	Me(δ)	0.91	23.25	0.93	22.95
	Me(δ′)	0.86	21.47	0.88	21.27
Ile[7]	NH	7.66		7.70	
	CO		171.10		–
	H–C(α)	4.39	60.78	4.40	60.52
	H–C(β)	1.57	38.57	1.57	38.26
	H–C(γ)	1.49	25.30	1.50	24.95
	H′–C(γ)	1.15		1.15	
	Me(γ′)	0.96	15.73	0.96	15.47
	Me(δ)	0.85	10.91	0.87	10.64
Ile[8]	NH	7.38		7.40	
	CO		170.80		–
	H–C(α)	4.64	55.27	4.69	55.01
	H–C(β)	1.75	37.27	1.76	36.94
	H–C(γ)	1.52	24.23	1.53	24.79
	H′–C(γ)	1.05		1.05	
	Me(γ′)	0.81	16.48	0.82	16.20
	Me(δ)	0.78	12.15	0.80	11.87

[a]) The resonances misassigned in [5] are shown in bold. [b]) This work. [c]) Values taken from [5].

also prove the identity of both compounds. The ^1H spin systems of each of the residues were identified by TOCSY [8] spectra. Using HMQC [9] and HMQC-TOCSY [10] spectra, the ^{13}C resonances of every spin system were unequivocally identified. The sequencing of the peptide was obtained from an HMBC [11] spectrum, which also allowed for the assignment of the carbonyl resonances. The cross-peak from Pro^2*C*O to Tyr^{3}N*H* shows a covalent bond between Pro^2*C*O and Tyr^3*N*H, proving the cyclic structure of our synthetic compound. The ^1H and ^{13}C assignments in DMSO are available from the authors.

There are some important differences in the resonance assignments of synthetic **1** and those reported for natural **1** [5]. A significant deviation is found in the assignment of the C(α) and C(β) resonances of Pro^1 and Pro^2. From the HMQC-TOCSY spectrum (*Fig. 1*),

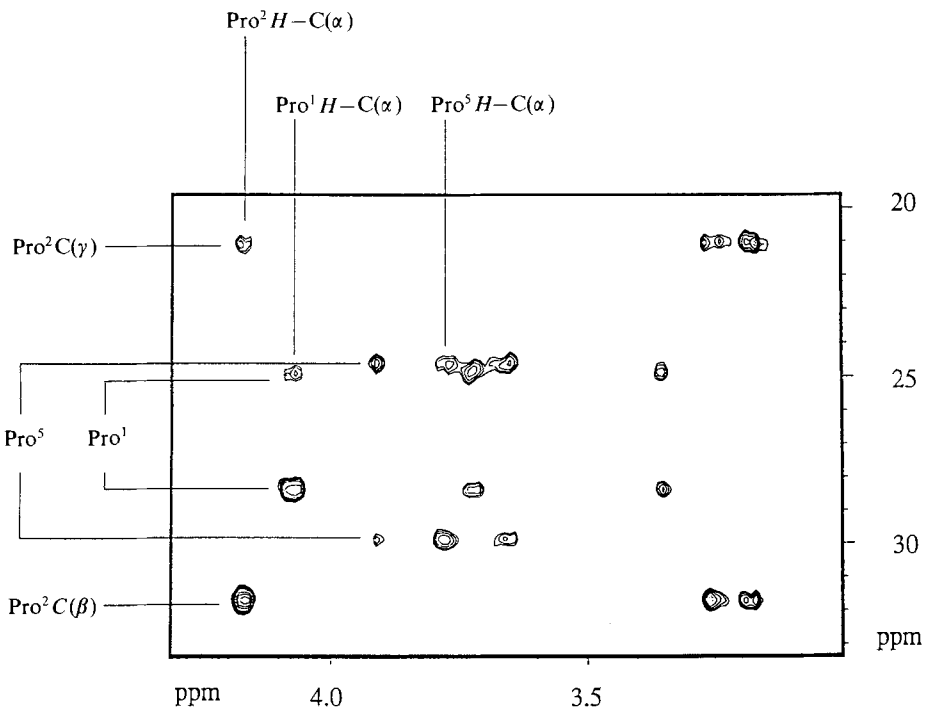

Fig. 1. *The C(β)/C(γ)* vs. H–*C(α)* /H–*C(δ) region of Pro residues in a HMQC-TOCSY spectrum of hymenistatin 1* (**1**) in $CDCl_3$ at 11.74 Tesla and 300 K, τ_{mix} 66 ms. Signals at 32.1 ppm (Pro^{2}C(β)) and 21.5 ppm (Pro^{2}C(γ)) belong to the same spin system (Pro^2: *e.g. H*(α) at 4.16 ppm).

the ^{13}C signals at 32.1 and 21.5 ppm can be unambiguously assigned to the same proline spin system, namely Pro^2. Additionally, we assigned the Tyr^{3}N*H* resonance to 7.26 ppm, very close to the residual signal from the solvent ($CHCl_3$ at 7.24 ppm), which may explain why it was not reported previously.

2.2.2. *Conformational Parameters.* The ^{13}C chemical shifts of C(β) and C(γ) of Pro residues are very sensitive to the configuration of the preceding peptide bond: a small difference between them (*ca.* 4–6 ppm) is indicative of a *trans*-configuration, while a

difference of 8–10 ppm is expected for a *cis*-configuration [12]. This configurational assignment was not possible with the NMR data published previously [5]. The corrected assignment of the resonances of Pro^1 and Pro^2 given above allows now to determine the amide-bond configuration of Pro^1-Pro^2 to be *cis*, while those between Ile^8-Pro^1 and Val^4-Pro^5 are *trans*.

Two other sets of resonances of very low intensity (< 5%) could be identified in $CHCl_3$. Exchange peaks between the different sets of resonances were observed in both the ROESY [13] and TOCSY [8] spectra (*Fig. 2*). The exchange peaks were unambiguously identified by the opposite phase compared to the ROE's in the ROESY. Because of the low concentration, the additional resonance sets could not be unambiguously assigned. Only one set of signals was observed in DMSO.

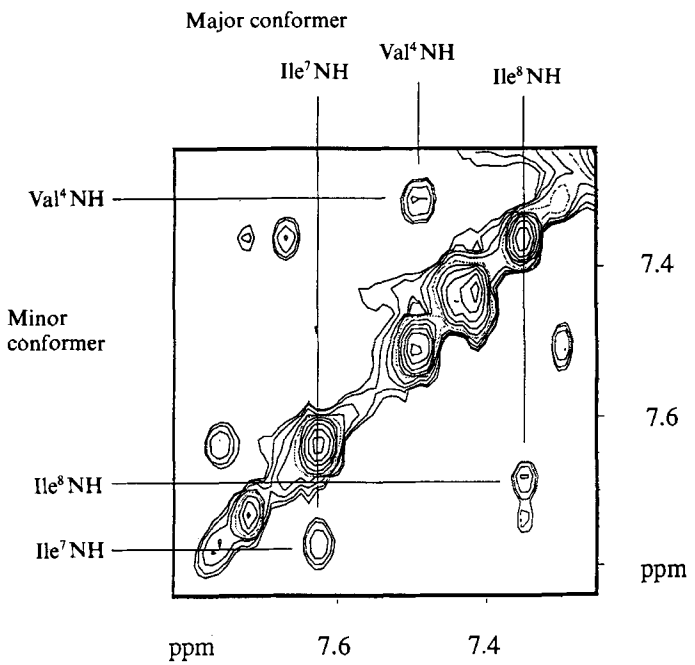

Fig. 2. *NH Region of the TOCSY spectrum of hymenistatin 1* (**1**). In $CDCl_3$ at 500 MHz and 300 K, τ_{mix} 80 ms. Exchange cross-peaks between NH's of the major and a minor conformation are illustrated (Val^4NH (major; 7.56 ppm)↔Val^4NH (minor; 7.31 ppm), Ile^7NH (major; 7.66 ppm)↔Ile^7NH (minor; 7.78 ppm), Ile^8NH (major; 7.38 ppm)↔Ile^8NH (minor; 7.68 ppm)).

The $^3J(NH,H-C(\alpha))$ homonuclear coupling constants were obtained from the one-dimensional ^{1}H-NMR spectrum. The $^3J(H-C(\alpha),H-C(\beta))$ coupling constants of Tyr^3 were obtained from an E.COSY [14]. All coupling constants are listed in *Table 3*. NOESY [15] ($CDCl_3$) and ROESY [13] (DMSO) spectra were recorded with a mixing time of 150 ms and 136 ms, respectively, to calculate the H–H distances of **1** in solution.

The temperature and concentration dependence of the chemical shifts of the amide protons were examined. The temperature coefficients listed in *Table 3* indicate that the amide groups of Val^4 and Ile^8 are buried (maybe involved in intramolecular H-bonds, see

Table 3. *Coupling Constants and Temperature Coefficients Measured for Hymenistatin 1* (**1**) *in $CHCl_3$ and DMSO*

Residue	Solvent	$-\Delta\delta/\Delta T$ [ppb/K]	^3J(NH,H–C(α)) [Hz]	^3J(H–C(α),$H_{pro\text{-}S}$–C(β)) [Hz]	^3J(H–C(α),$H_{pro\text{-}R}$–C(β)) [Hz]
Pro[1]	$CHCl_3$			7.7	5.2
	DMSO			9.4	3.1
Pro[2]	$CHCl_3$			9.7	< 1
	DMSO			–	–
Tyr[3]	$CHCl_3$	4.0	5.7	4.6	12.8
	DMSO	2.4	6.6	4.7	12.2
Val[4]	$CHCl_3$	–2.2	9.7	10.1	
	DMSO	–0.1	9.7	10.3	
Pro[5]	$CHCl_3$			7.3	9.6
	DMSO			6.3	7.8
Leu[6]	$CHCl_3$	11.0	br.	4.8	9.8
	DMSO	6.1	6.8	8.7	11.8
Ile[7]	$CHCl_3$	4.0	8.9	8.8	
	DMSO	0.1	8.9	8.8	
Ile[8]	$CHCl_3$	–0.4	8.5	7.7	
	DMSO	3.1	7.8	7.2	

below). In contrast, the amide group of Leu[6] has a large temperature coefficient and is also strongly dependent on concentration. It is, therefore, directed towards the solvent and may even be involved in an intermolecular H-bond, at higher concentrations.

2.3. *MD Simulations.* 2.3.1. *General.* The conformation of hymenistatin 1 (**1**) was examined by MD simulations. For the $CHCl_3$ study, the distance restraints were obtained from 61 NOE signals: 32 intra-residue, 22 sequential, 5 medium range, and 2 reference cross-peaks. Distances were calculated using the two well separated geminal H–C(β) of Tyr[3] as a standard, assuming a distance of 178 pm. The calibration was verified by calculating the distance between the *ortho*- and *meta*-protons in the aromatic ring of Tyr[3] (203 pm). The remaining 59 distances were used as restraints as given in *Table 4*. In addition, coupling-constant restraints were applied as previously described [16] for the ^3J(NH,H–C(α))'s measured for Tyr[3], Val[4], Ile[7], and Ile[8] and the ^3J(H–C(α),H–C(β))'s measured for Tyr[3], Val[4], Leu[6], Ile[7], and Ile[8].

In DMSO, 61 ROE's were observed: 26 intra-residue, 25 sequential, and 10 medium range. A similar procedure was used for calculating distances. Coupling-constant restraints were applied for all of the couplings listed above for $CHCl_3$ with the addition of ^3J(NH,H–C(α)) for Leu[6] (see *Table 3*).

The starting structure for the simulations was created by application of a forcing potential to all dihedral angles to 180° (except for the ω dihedral between Pro[1]-Pro[2] which was set to 0°) and energy minimization. The cyclic peptide can not, of course, adopt a structure that meets this artificial forcing and, therefore, a conformation of high energy is produced, with an almost circular arrangement of the backbone with no secondary structure elements (*i.e.* H-bonds or turns). To eliminate artifacts from *in vacuo* calculations, all simulation were preformed using the appropriate solvent box. After the MD run with distance and coupling-constant restraints, the stability of the restrained structure was examined by continuing the simulation without experimental restraints (*i.e.* a free MD simulation starting from a structure that fulfills the NMR observables).

Table 4. *Distances* [pm] *Calculated from NOESY and ROESY Spectra and the Average Values During the MD Simulations of Hymenistatin 1* (**1**) *in $CHCl_3$ and DMSO*

Atoms[a])		$CHCl_3$		DMSO	
		NOE	MD	ROE	MD
Inter-residue					
Pro^1H–C(α)	Pro^2H–C(α)	173	190	205	170
Pro^1H–C(α)	Tyr^3NH	283	259	253	293
Pro^1H–C(α)	Val^4NH	307	342	266	326
Pro^1H–C(α)	Ile^8NH	433	488	390	402
Pro^1H–C(α)	Pro^5H–C(α)			300	265
$Pro^1H_{pro\text{-}R}$–C(β)	Pro^2H–C(α)			260	283
$Pro^1H_{pro\text{-}S}$–C(β)	Pro^2H–C(α)			292	283
$Pro^1H_{pro\text{-}S}$–C(β)	$Pro^2H_{pro\text{-}R}$–C(δ)			**301**	**417**
$Pro^1H_{pro\text{-}S}$–C(β)	Pro^5H–C(α)			281	300
$Pro^1H_{pro\text{-}S}$–C(β)	Leu^6NH			389	439
$Pro^1H_{pro\text{-}R}$–C(δ)	Leu^6NH			365	353[b])
$Pro^1H_{pro\text{-}R}$–C(δ)	Ile^7NH			314	331
$Pro^1H_{pro\text{-}R}$–C(δ)	Ile^8NH	331	266	294	296
$Pro^1H_{pro\text{-}R}$–C(δ)	Ile^8H–C(α)	291	239	257	293
$Pro^1H_{pro\text{-}S}$–C(δ)	Ile^8NH	408	363	**300**	**386**
$Pro^1H_{pro\text{-}S}$–C(δ)	Ile^8H–C(α)	245	220	214	222
Pro^2H–C(α)	Tyr^3NH			331	302
Pro^2H–C(α)	Ile^8NH			458	554
$Pro^2H_{pro\text{-}R}$–C(δ)	Tyr^3H–C(3′),H–C(5′)	348	493[b])		
$Pro^2H_{pro\text{-}S}$–C(δ)	Tyr^3NH	314	315	286	349
$Pro^2H_{pro\text{-}S}$–C(δ)	Tyr^3H–C(2′),H–C(6′)	332	397[b])	301	472[b])
$Pro^2H_{pro\text{-}S}$–C(δ)	Tyr^3H–C(3′),H–C(5′)	298	348[b])	306	458[b])
Tyr^3NH	Val^4NH	258	274	282	273
Tyr^3H–C(α)	Val^4NH	353	362	327	355
$Tyr^3H_{pro\text{-}R}$–C(β)	Val^4NH	265	217	247	321
$Tyr^3H_{pro\text{-}S}$–C(β)	Val_4NH	349	345	255	221
Tyr^3H–C(3′),H–C(5′)	Ile^8H–C(α)	414	720[b])		
Val^4NH	Ile^8NH	**258**	**417**	369	353
Val^4H–C(α)	$Pro^5H_{pro\text{-}R}$–C(δ)	239	232	229	225
Val^4H–C(α)	$Pro^5H_{pro\text{-}S}$–C(δ)	248	236	218	240
Pro^5H–C(α)	Leu^6NH	**244**	**344**	223	215
Pro^5H–C(α)	Ile^7NH	400	443	375	382
Leu^6NH	Ile^7NH	240	271	298	341
Leu^6H–C(α)	Ile^7NH	353	353	341	340
$Leu^6H_{pro\text{-}S}$–C(β)	Ile^7NH	373	369		
Ile^7NH	Ile^8NH	237	289	230	254
Ile^7H–C(α)	Ile^8NH	**375**	**259**	341	353
Ile^7H–C(β)	Ile^8NH			**232**	**363**
Intra-residue					
Pro^1H–C(α)	$H_{pro\text{-}R}$–C(β)	310	298	294	290
Pro^1H–C(α)	$H_{pro\text{-}S}$–C(β)	267	239	229	240
Pro^1H–C(α)	$H_{pro\text{-}R}$–C(γ)	328	313		
Pro^2H–C(α)	$H_{pro\text{-}R}$–C(β)	253	282		
Pro^2H–C(α)	$H_{pro\text{-}S}$–C(β)	264	243		
Tyr^3NH	H–C(α)	292	278	280	278
Tyr^3NH	$H_{pro\text{-}R}$–C(β)	290	261	**253**	**342**
Tyr^3NH	$H_{pro\text{-}S}$–C(β)	339	355	237	224
Tyr^3NH	H–C(2′),H–C(6′)	259	264[b])	263	268[b])

Table 4 (cont.)

Atoms[a])		$CHCl_3$		DMSO	
		NOE	MD	ROE	MD
Tyr^3H–C(α)	$H_{pro\text{-}R}$–C(β)	324	300		
Tyr^3H–C(α)	$H_{pro\text{-}S}$–C(β)	263	237	237	254
Tyr^3H–C(α)	H–C(2′),H–C(6′)	271	289[b])	245	278[b])
Tyr^3H–C(α)	H–C(3′),H–C(5′)	403	518[b])		
$Tyr^3H_{pro\text{-}R}$–C(β)	H–C(2′),H–C(6′)	257	213[b])	231	214[b])
$Tyr^3H_{pro\text{-}R}$–C(β)	H–C(3′),H–C(5′)	434	466[b])		
$Tyr^3H_{pro\text{-}R}$–C(β)	$H_{pro\text{-}S}$–C(β)	178[c])		178[c])	
$Tyr^3H_{pro\text{-}S}$–C(β)	H–C(2′),H–C(6′)	269	213[b])	280	214[b])
$Tyr^3H_{pro\text{-}S}$–C(β)	H–C(3′),H–C(5′)			429	471[b])
Tyr^3H–C(2′),H–C(6′)	H–C(3′),H–C(5′)	204[c])		208[c])	
Val^4NH	H–C(α)	307	292	281	295
Val^4NH	H–C(β)	296	267	249	266
Val^4H–C(α)	H–C(β)	306	294	274	295
Pro^5H–C(α)	$H_{pro\text{-}R}$–C(β)	289	301		
Pro^5H–C(α)	$H_{pro\text{-}S}$–C(β)	264	241	232	244
Leu^6NH	H–C(α)	252	273	242	206
Leu^6NH	$H_{pro\text{-}R}$–C(β)	318	254	336	347
Leu^6NH	$H_{pro\text{-}S}$–C(β)			**309**	**395**
Leu^6H–C(α)	$H_{pro\text{-}R}$–C(β)	309	301		
Leu^6H–C(α)	$H_{pro\text{-}S}$–C(β)	285	253	245	256
Ile^7NH	H–C(α)	319	289	279	287
Ile^7NH	H–C(β)	293	277	239	238
Ile^7H–C(α)	H–C(β)	302	292	251	299
Ile^8NH	H–C(α)	308	223	280	294
Ile^8NH	H–C(β)	344	366	229	276
Ile^8H–C(α)	H–C(β)	287	295	233	295
Ile^8H–C(α)	H–C(γ)	317	292	272	275

[a]) For the upper and lower distant restraint, 10% was added or subtracted. The distance restraints with a violation of more than 50 pm from these restraints are shown in bold.

[b]) The upper distance restraint was increased by 220 pm.

[c]) Distances used for calibration.

2.3.2. *Conformation in $CHCl_3$.* The average values of the dihedral angles from the MD simulation in $CHCl_3$ are given in *Table 5*. The overall conformation can be described as a pseudo-β strand, extending from Pro^2-Pro^5 on one side and Leu^6-Pro^1 on the other. There are turns at both ends: a well defined βVIa turn [17] about Pro^1-Pro^2 and a βI between Pro^5-Leu^6. Intramolecular H-bonds are found between Tyr^3NH and Ile^8CO as part of the βVIa turn, between Ile^7NH and Val^4CO as part of the βI turn, and between Val^4NH and Ile^8CO (for 89% of the simulation) and Ile^7CO (for 38% of the simulation). The pseudo-β strand is not flat and extended, but adopts a 'twisted banana' conformation. There are NOE's observed between the two ends (*i.e.* Pro^1-H–C(α)/Val^4NH) which cause the molecule to fold up and slightly twist. The NOE distance-restraint violation during the restrained simulation is 12 pm. Only three of the restraints have violations greater than 50 pm, shown in bold in *Table 4*, and involve regions of the molecule which undergo conformational changes in DMSO, as discussed below. The partially minimized average conformation of **1** from the MD simulation in $CHCl_3$ is shown in *Fig. 3a*.

Table 5. *Averages of Dihedral Angles* [°] *of Hymenistatin 1* (**1**) *in $CHCl_3$ and DMSO from Restrained and Free Molecular-Dynamics Simulations*[a])

Torsion[a])		$CHCl_3$		DMSO		Torsion[a])		$CHCl_3$		DMSO	
		NOE	free	NOE	free			NOE	free	NOE	free
Pro^1	ϕ	–63	–62	–64	–67	Pro^5	ϕ	–49	–48	–44	–48
	ψ	144	144	153	138		ψ	**–41**	**–43**	**139**	**138**
	χ_1	–16	–20	10	–6		χ_1	–22	–23	–32	–18
	χ_2	20	25	–17	10		χ_2	23	25	36	20
	χ_3	–16	–20	17	–10		χ_3	–15	–18	–28	–15
	χ_4	7	8	–12	7		χ_4	1	3	8	5
Pro^2	ϕ	–87	–86	–91	–77	Leu^6	ϕ	**–74**	**–73**	**66**	**69**
	ψ	10	2	*23*	*–48*		ψ	–43	–55	–28	–45
	χ_1	22	25	28	–10		χ_1	–62	–97	–61	–97
	χ_2	–15	–23	–33	21						
	χ_3	3	12	27	–25	Ile^7	ϕ	–120	–103	–88	–72
	χ_4	11	5	–10	20		ψ	**70**	**90**	**–63**	**–64**
							χ_1	–38	–48	–58	–54
Tyr^3	ϕ	–71	–62	*–69*	*3*		χ_2	170	121	140	127
	ψ	–61	–63	–50	–74						
	χ_1	–45	–57	–66	–55	Ile^8	ϕ	**80**	**63**	**–132**	**–127**
							ψ	108	96	75	92
Val^4	ϕ	–138	–126	–127	–120		χ_1	–56	–56	–53	–31
	ψ	135	127	96	106		χ_2	138	136	131	138
	χ_1	–55	–61	–51	–28						

[a]) Torsions which differ by more than 50° in the restrained and free simulation are shown in italics (see text), those responsible for different conformations in bold.

2.3.3. *Conformation in DMSO.* The overall conformation of **1** in DMSO (*Fig. 3b*) is similar to that found in $CHCl_3$ (compare dihedral angles in *Table 5*). The two major differences are a 150° rotation of the amide bond between Ile^7 and Ile^8 (see ψ of the Ile^7 and ϕ of the Ile^8 in *Table 5*) and the preference of a βII turn about Pro^5-Leu^6. The switching of the peptide bond between Ile^7 and Ile^8 also causes a slight distortion of the βVIa turn about Pro^1-Pro^2. In fact, the H-bond associated with this turn, Tyr^3NH-Ile^8CO, is only found during a small portion of the simulation (10%). Instead a H-bond between Tyr^3NH and Pro^1CO (consistent with a γ turn about Pro^2) is observed for 89% of the simulation. The NH of Ile^8 projects towards the peptide, forming an intramolecular H-bond to Val^4CO. Despite these H-bonding patterns, the average dihedral angles of Pro^1 and Pro^2 are in agreement with those reported for standard βVIa turns [17]. The Val^4NH is involved in a H-bond with Ile^8CO. Concerning the other 'half' of the molecule, the average dihedral angles are in good agreement with the standard values for a βII turn. The H-bond about this turn, Ile^7NH-Val^4CO, is observed for 59% of the simulation. Again a H-bond, Ile^7NH-Pro^5CO, consistent with a γ-turn is present during a large portion of the simulation (89%). The apparent existence of both the β and γ turns indicates dynamics taking place during the simulation. The interconversion between a 'pure' β turn and a γ turn is quite facile: the NH of the $(i + 3)$ residue needs only to rotate out of the plane of the ten-membered H-bond-containing ring towards the carbonyl of the $i + 1$ residue (*i.e.* the ϕ and ψ of the $i + 2$ residue change from 80°, 0° to 70°, –50°. It is

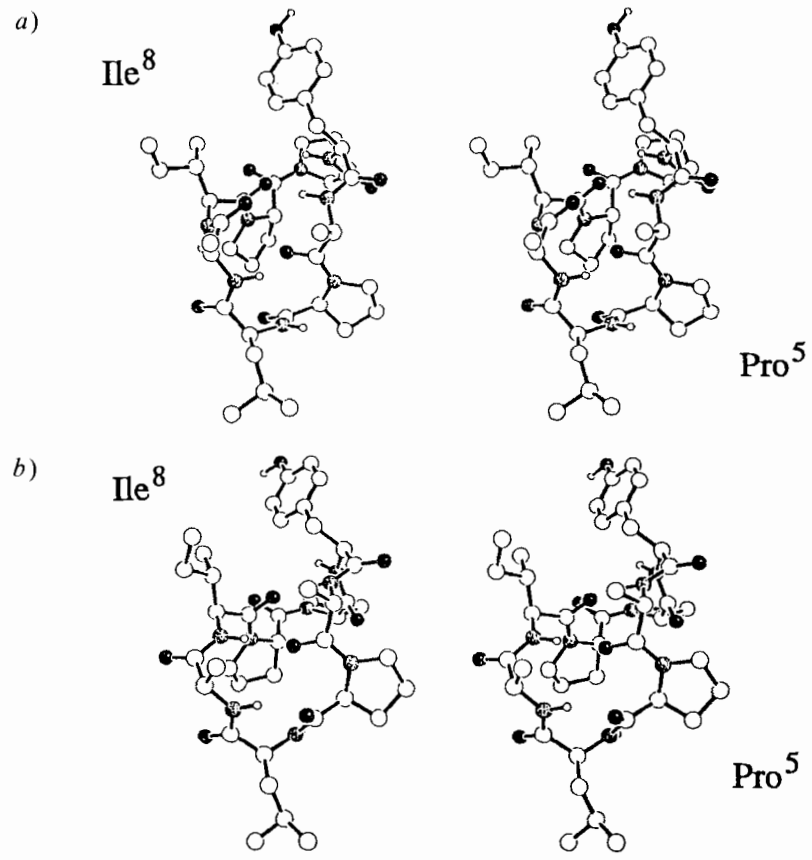

Fig. 3. *Structures of hymenistatin 1* (**1**) *in* a) *$CHCl_3$ and* b) *DMSO, averaged from free MD simulation* (200 ps) *at 300 K.* Only the C(β) of the side chains of Val^4 and Ile^7 are shown for clarity. The amide bonds between Pro^5-Leu^6 (bottom of figures) and Ile^7-Ile^8 (top left of figures) differ by 180° in the two solvents. Also the Pro^2-Tyr^3 amide bond is slightly twisted.

important to stress the difference observed in $CHCl_3$ and DMSO (*i.e.* the switching between a βI and βII turn) which is discussed below in *Chapt. 2.3.5.* The average distance-restraint violation during the MD is 10 pm, and there are five restraints with violations greater than 50 pm shown in bold in *Table 4.* The partially energy minimized average structure from the MD is shown in *Fig. 3b.*

2.3.4. *Free MD Simulations.* Free MD simulations, in the same solvent as used for the experimental measurements, were shown to be a good measure of the quality of the determined structure [18]. The restraints, distance and coupling constants, are simply turned off, and the simulation is then allowed to continue for an extended period (here 200 ps). The first portion of the simulation is to equilibrate the molecule to the lack of restraints. Such simulations will also indicate the application of experimental restraints that are not energetically favorable (as determined from the force field).

The results from the free MD of hymenistatin 1 (**1**) in $CHCl_3$ and DMSO are given in *Table 5.* In $CHCl_3$, there are only minor changes observed in the dihedral angles (the

largest deviation for a backbone torsion is 20°). The rms difference between the average structures from the restrained and free portions of the simulations is 57 pm for all heavy atoms (34 pm for the backbone). In DMSO, there are changes in the Pro^2 ψ and Tyr^3 ϕ dihedral angles (a change of *ca.* 60°) during the free MD, indicating possible dynamics about the βVIa turn. This is in accord with a study of a series of model peptides, where the βVI turns were found to vary greatly in the ψ dihedral of the $i + 2$ residue (here Pro^2) [17b]. In DMSO, the Pro^1 ring system shows greater dynamics during the free MD. The standard deviations of these dihedrals (data not shown) are *ca.* 20°, indicating a fluctuation between the two envelope conformations, while Pro^2 switches from one envelope conformation to the other. The rms difference for the restrained and free MD is 77 pm for the heavy atoms (36 pm for the backbone atoms).

2.3.5. *Solvent Interactions from MD Simulations.* The intermolecular interactions between the solvent and peptide can be examined by the calculation of pairwise atomic radial distribution functions (rdf's) [19]. The atom-atom rdf is a measure of the pairwise distribution of atoms, normalized by the density of the atoms in the pure solvent. We previously used rdf's in the analysis of the conformation of cyclic peptides from DMSO simulations [20]. The atomic rdf of the amide N-atom and the O-atom of the DMSO clearly illustrate intermolecular H-bonds. This is shown for the amide groups of Val^4, Leu^6, and Ile^7 in *Fig. 4*. The amide group of Leu^6 is projecting into the solvent, and the well defined peak at 0.28 nm, integrating to *ca.* 1 DMSO molecule, is an indication of an

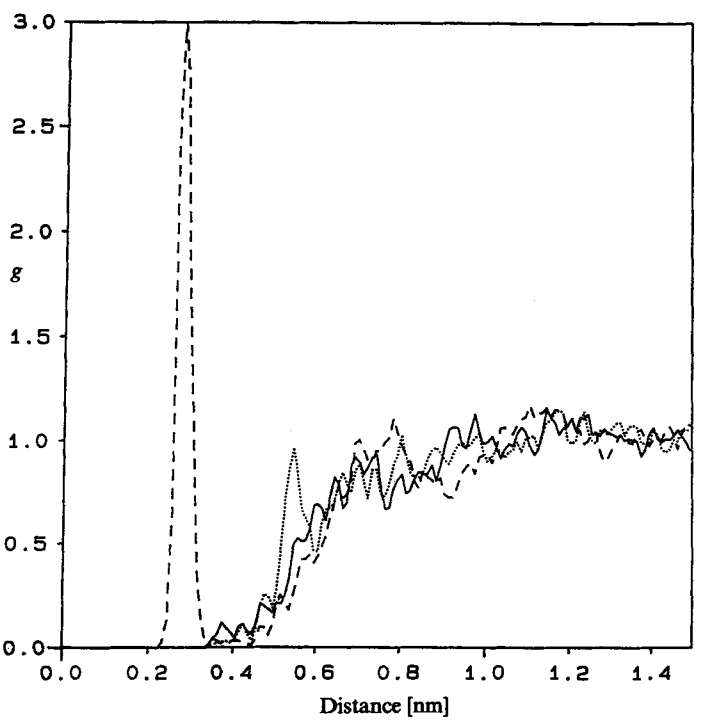

Fig. 4. *Atom-atom radial distribution functions calculated between the S-atom of DMSO and the amide N-atom of* Val^4 (—), Leu^6 (– – –), *and* Ile^7 (· · · ·) *from the MD simulation of the hymenistatin 1* (**1**) *in DMSO*

intermolecular H-bond between the solvent and peptide. In contrast, the amide protons of Val[4] and Ile[7] that are projecting away from the solvent, are involved in intramolecular H-bonds. The rdf's show no ordered solvent, slowly approaching a value of one, indicating a distribution of pure solvent (the rdf's slowly increase because of the exclusion of the solvent by the remainder of the peptide, which has not been taken into consideration).

The amide N-atom to solvent rdf's for the $CHCl_3$ simulations show very small differences between those amide groups that are projecting into the solvent and those forming intramolecular H-bonds (see *Fig. 5a*). This is to be expected since $CHCl_3$ is not a good H-bond acceptor. On the other hand, the rdf's of the O-atom of the CO groups of the peptide and the solvent are quite illustrative. They are shown in *Figs. 5b* and *5c*. For those CO groups projecting into the solvent, there is a large first peak at *ca.* 0.28 nm which integrates to *ca.* 1 solvent molecule. This is the case for the CO groups of Pro[2] (*Fig. 5b*, – – –), Tyr[3] (*Fig. 5b*, · · · · ·), and Leu[6] (*Fig. 5c*, ——). In contrast, the rdf's for those CO groups involved in intramolecular H-bonds show no well defined peaks, just a gradual increase (from *ca.* 0.4 to 0.9 nm) to a value of one (see Val[4] in *Fig. 5b*, ——). Even the partial interaction of the CO group with the solvent can be seen by a peak of the same shape but smaller intensity (see Ile[7] in *Fig. 5c*, – – –). The rdf's include oscillations because of the limited number of structures (1 structure/ps) stored during the simulation and have not been smoothed [19].

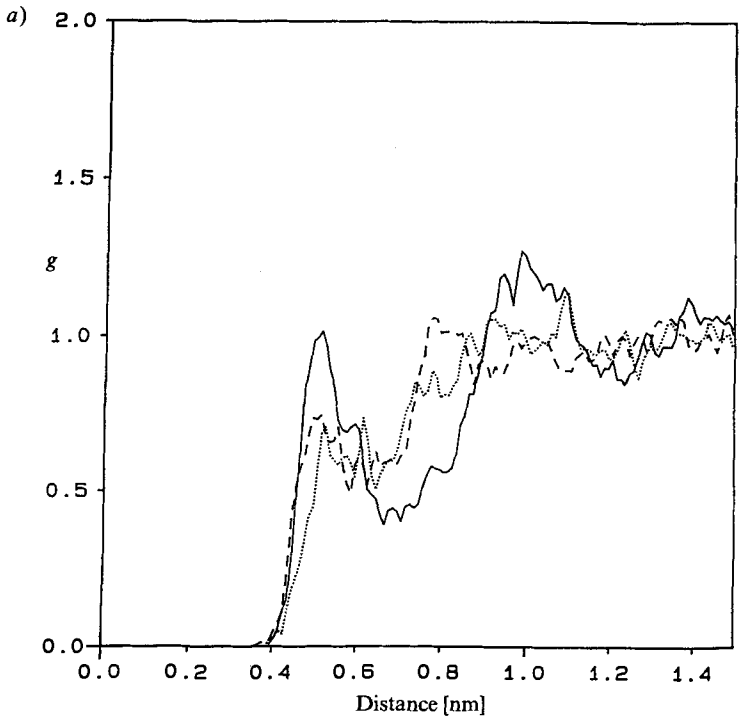

Fig. 5. *Atom-atom radial distribution functions calculated between the C-atom of chloroform and* a) *the amide N-atom of Val[4]* (——), *Leu[6]* (– – –), *and Ile[7]* (· · · · ·), b) *the carbonyl O-atom of Pro[2]* (– – –), *Tyr[3]* (· · · · ·), *and Val[4]* (——), *and* c) *the carbonyl O-atom of Pro[5]* (· · · · ·), *Leu[6]* (——), *and Ile[7]* (– – –) *from the MD simulation of the hymenistatin 1* (**1**) *in* $CHCl_3$

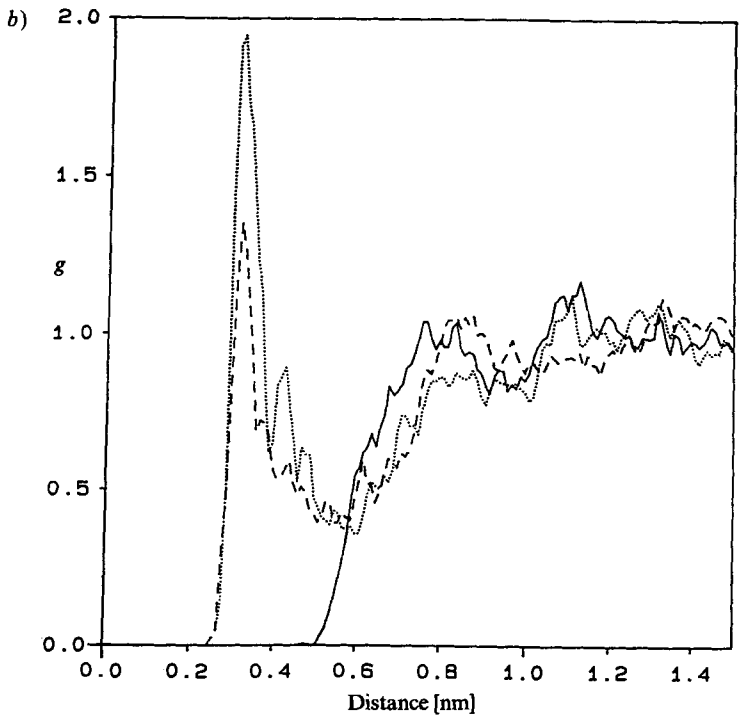
b)
2.0
1.5
g
1.0
0.5
0.0
0.0
0.2
0.4
0.6
0.8
1.0
1.2
1.4
Distance [nm]

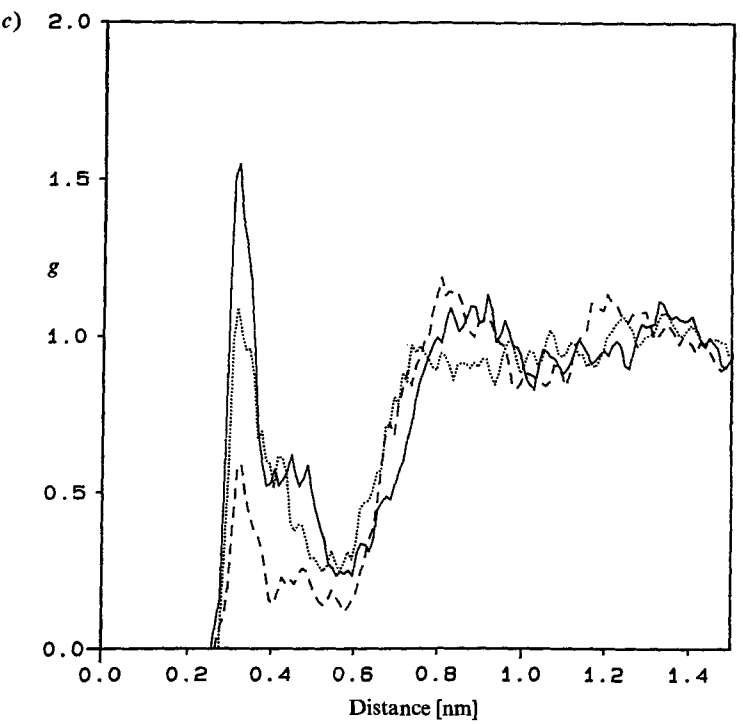
c)
2.0
1.5
g
1.0
0.5
0.0
0.0
0.2
0.4
0.6
0.8
1.0
1.2
1.4
Distance [nm]

2.3.6. *Conformational Differences in $CHCl_3$ and DMSO.* The differences observed in the MD simulations of **1** in $CHCl_3$ and DMSO are clearly in accord with the NOE's. In DMSO, there is an important NOE involving Ile^{8}N*H* (Ile^{8}N*H*/Pro^2*H*–C(α)) which is not present in $CHCl_3$. In addition, the derived distances between Ile^{8}N*H* and Pro^1*H*–C(α) and *H*–C(δ) are shorter in DMSO than in $CHCl_3$. This indicates that N*H* of Ile^8 is directed away from the solvent, towards the middle of the peptide. This difference can be explained by examination of the $CHCl_3$ structure. Because of the weaker interaction of the solvent with the peptide ($CHCl_3$ is less polar than DMSO), there is a tendency to form intramolecular H-bonds. This can be see for Ile^{8}N*H* and Leu^{6}C*O*, forming a γ-turn about Ile^7. Such interactions are less favored in more polar solvents and, therefore, not observed in DMSO.

The other major difference in conformation is the β-turn about Pro^5-Leu^6. Again, the NOE's can account for the observed differences. The most important are NOE's between Leu^{6}N*H* and the *H*–C(β) and *H*–C(δ) of Pro^1 which are observed only in DMSO. In addition, the Leu^{6}N*H* and ILe^{7}N*H* distance is longer in DMSO (300 pm compared with 233 pm in $CHCl_3$). This partially accounts for the observation of the γ-turn about Leu^6 during the simulation in DMSO (see discussion above), the distance for a βII turn is 240 pm. This difference in conformation must arise from solvent effects. As shown above (*Figs. 4* and *5*), $CHCl_3$ interacts strongly with CO groups, while the DMSO forms intermolecular H-bonds with the amide protons [20]. In $CHCl_3$, the CO of Pro^5 has a contact area more than 3 times greater than in DMSO (5.2 compared with 1.6 Å^2). This was achieved by measuring the solvent exposure for the amide and carbonyl moieties (*i.e.* the contact area) following standard procedures [21]. The solvent exposure of the Pro^5 CO group is illustrated in *Fig. 6*.

Consequently, the amide proton of Leu^6 is completely shielded from the solvent in $CHCl_3$, while a contact area of 1.7 Å^2 is calculated in DMSO. Therefore, the solvent interactions with the peptide can be used to explain the different conformations. This difference is shown in *Fig. 7*.

It is important to remark that despite the differences noted above, the general conformation of the peptide in the two solvents is similar. This can be illustrated by calculation of the distance-restraint error using the NOE restraints measured in DMSO and the structure obtained from the MD simulation in $CHCl_3$ (and *vice versa*). A restraint violation of 42 pm is calculated for the partially minimized average structure from the $CHCl_3$ simulation when using the NOE's from DMSO, a value of 46 pm is calculated for the average structure from DMSO and the NOE's from $CHCl_3$. The rms difference between the average structures from the $CHCl_3$ and DMSO simulations is 0.20 nm when using all heavy atoms (0.13 nm for the backbone atoms). However, the residues 1–4 superimpose almost perfectly (rms 0.03 nm).

2.4. *Biological Results.* Hymenistatin 1 (**1**) was tested for inhibition of colony formation in soft agar of L1210 mouse leukaemia cells, KB human epidermoid carcinoma cells, and mouse bone marrow cells stimulated by GM-CSF. In none of the systems was inhibition of colony formation found, up to the maximal test concentration of 10 µg/ml. Likewise, when tested for cytotoxicity against P388 mouse leukaemia cells in the MTT-assay, **1** had no effect up to a concentration of 1 µg/ml. We found no effect of **1** on the growth of tumor cells or normal bone marrow cells. This seems to be in contrast to the reported activity of **1** against P388 cells [5]. However, in the assays with long incubation

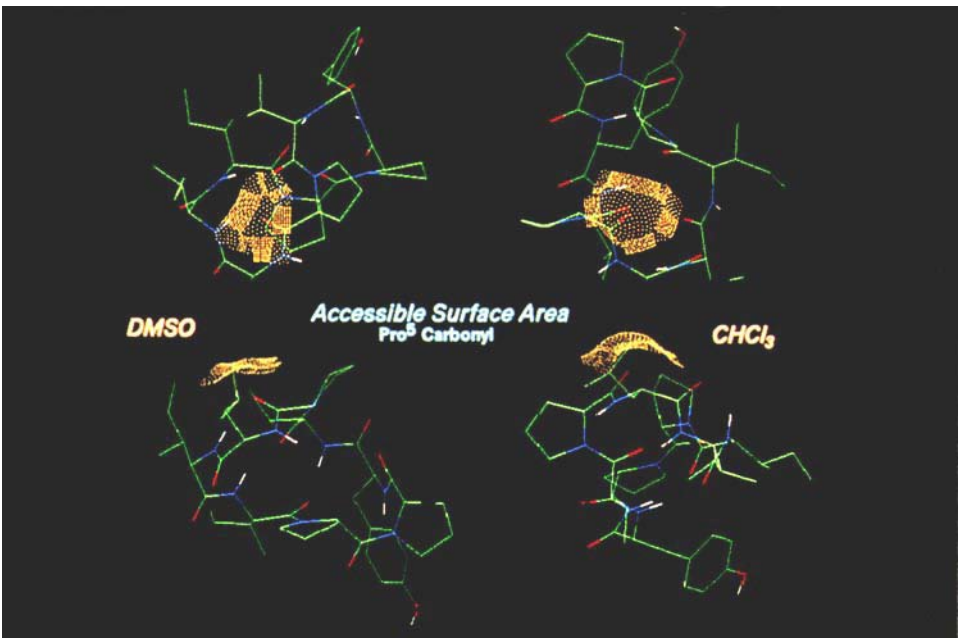

Fig. 6. *Accessible surface area of the Pro^5 CO group* (left: DMSO, right: $CHCl_3$)

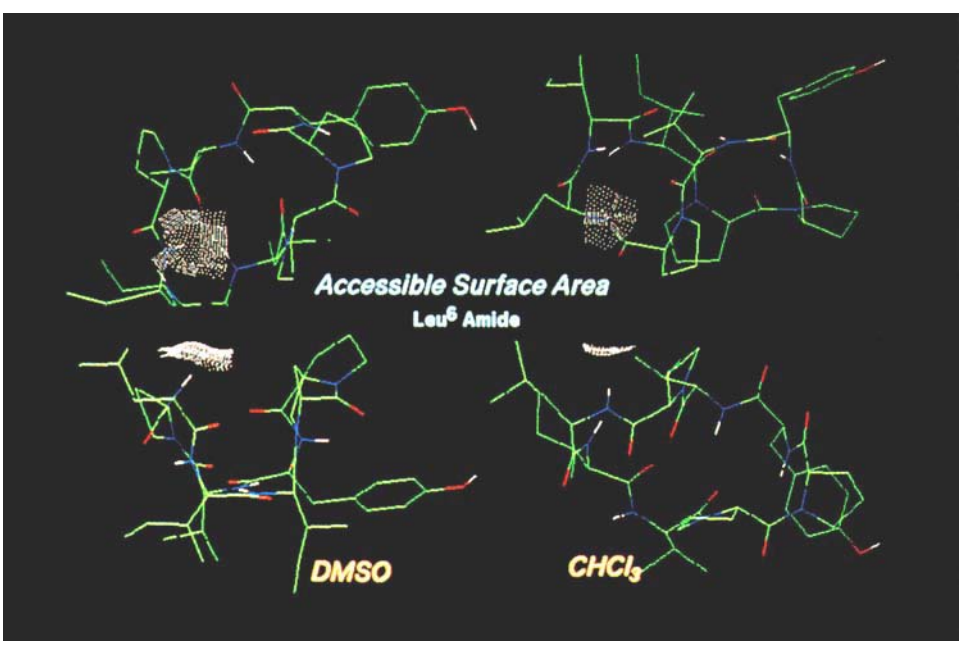

Fig. 7. *Accessible surface area of the Leu^6 anide group* (left: DMSO, right: $CHCl_3$)

periods, other cell lines were used by us. In our assay for cytotoxicity against P388 murine leukaemia cells, the cells were incubated for a maximum of 48 h in the presence of test substance. Therefore, we can not conclude that our results do not agree with the reported activity of **1**. In addition, the reported cytotoxic concentrations (3.5 μg/ml) are in the same range as the maximum concentration tested by us, so that variations in test design and cell line can account for the observed differences.

Experimental Part

General. The amino acids were provided from *Degussa AG*. Boc-Amino acids were synthesized using di(*tert*-butyl) carbonate from *Fluka*. BtOH (= 1*H*-benzotriazol-1-ol) was synthesized from 2-chloronitrobenzene (from *EGA-Chemie*) and hydrazine hydrate (from *Merck-Schuhardt*). CF_3COOH was obtained from *Kali-Chemie*, methanesulfonic acid (MsOH) from *Riedel-de-Haën*, isopentyl nitrite and *N,N'*-dicyclohexylcarbodiimide (DCC) from *Fluka*. All solvents were distilled before use. Gel filtration: *Sephadex LH20* column with *Thorn 243* (optical rotation) and *Uvicord II* (UV absorption) flow detectors; MeOH as eluent. Optical rotations: *241-Perkin-Elmer* polarimeter; at r.t. at 589 nm. IR Spectra: *841-Perkin-Elmer* spectrometer; KBr matrix. FAB-MS: *Varian-MAT-311A* spectrometer; recorded in the Laboratorium für Strukturchemie, TU München; nitrobenzyl alcohol (NBA) as matrix.

Esterification. At 55°, 10 g of 1% chloromethylated *Merrifield*'s resin was added to 17.36 g (50 mmol) of Boc-Pro-OCs in 100 ml of *N,N*-dimethylacetamide and shaken for 10 d at 55°. Boc-Pro-resin (11.58 g) was obtained with an occupation of 0.76 mmol/g.

Solid-Phase Synthesis. The synthesis was carried out with 5.45 g (4 mmol) of the resin and coupling of Boc-protected amino-acid derivates (2.5 equiv.) with BtOH (10 mmol) and DCC (10 mmol). Deprotection was achieved with a soln. of 10% CF_3COOH and 0.25% MsOH in CH_2Cl_2 for over 30 min. An 11% $(i\text{-}Pr)_2EtN$ soln. in CH_2Cl_2 was used for neutralization. Coupling times were: 2.5 h for Pro^1, Tyr^3, Pro^5, and Ile^7, 3 h for Leu^6, and 4 h for Val^4 and Ile^8. Coupling was monitored by a ninhydrin test [22] and additionally by an isatin test (specific for prolines) [23] after coupling of Pro^1, Ile^8, and Val^4.

Hydrazinolysis was achieved by shaking the resin with 20% $NH_2NH_2 \cdot H_2O$ in *N,N*-dimethylacetamide for 65 h at r.t. producing 1.55 g (38%) of the linear peptide. M.p. 180°. $[\alpha]_D = -88.24$ ($c = 1$, DMF). TLC ($BuOH/AcOH/H_2O$ 3:1:1): R_f 0.71.

Deprotection of the N-terminal tyrosine of the linear peptide was achieved by dissolving in 6 ml of CH_2Cl_2, adding 10 ml of CF_3COOH, 140 μl of scavenger (ethane-1,2-dithiol), and treating the mixture for 20 min in an ultrasonic bath producing 1.76 g (100%) of the N-terminal deprotected peptide. M.p. 205° (dec.). $[\alpha]_D = -75.88$ ($c = 1$, DMF). TLC ($AcOEt/CHCl_3/MeOH$): R_f 0.46.

Cyclization (azide method). The linear peptide was dissolved in a brown-glass flask in 4 ml of DMF and cooled to −30°. Then 612 μl of conc. HCl soln. and 306 μl of isopentyl nitrite were added. The mixture was stirred for 90 min at −15° (azide identification by IR (2140 cm^{-1})). This mixture was added into 1 l of cold (−18°) DMF, and $(i\text{-}Pr)_2EtN$ was added until a pH of 9 was reached. After 7 d at 4° in the dark, the volatile compounds were evaporated. The oil was dissolved in $MeOH/H_2O$ 5:1, and 40 g of mixed bead ion exchanger were added.

Purification. The crude product was purified by short-column chromatography (silica gel *60* (0.063–0.2 mm), $CHCl_3$/MeOH 9:1) and flash chromatography (silica gel *60* (0.032–0.063 mm), (−)-(*S*)-ethyl lactate/i-PrOH 1:1) producing 750 mg of **1** contaminated with eluent. Gel filtration (*Sephadex LH 20*, MeOH) produced 187 mg (14%) of **1**. Final purification was carried out by HPLC (*Beckmann* instrument, mod. *420* controller, mod. *1108* solvent delivery unit; semi-prep. *C18* column from *Macherey-Nagel* (250 × 1 × 7); *Knaur Uvicord* (220 nm) detector; H_2O (0.11%/CF_3COOH) and MeCN (0.09% CF_3COOH), gradient of 50→90% in 20 min; flow rate 6 ml/min). TLC ($CHCl_3$/MeOH 9:1): R_f 0.16.

Alternative Synthesis of **1**: *Cyclization of the Linear Precursor H-Ile-Ile-Pro-Pro-Tyr-Val-Pro-Leu-OH · HF.* The linear octapeptide was built up according to a standard solid-phase protocol with the semiautomatic synthesizer *SP 650* (*Labortec AG*, Switzerland), using a hydroxymethyl resin for C-terminal attachment of Boc-leucine, followed by successive coupling of Boc-amino acids in threefold excess of diisopropylcarbodiimide, BtOH, and protected amino acid in CH_2Cl_2/DMF. The linear peptide was cleaved from the polymeric support by treatment with liquid HF (60 min, 0°) to yield 2.21 g of almost homogeneous material, suitable for cyclization without further purification. Cyclization was carried out twice in similar batches using 0.93 g (1 mmol) of peptide, 1.92 g (10 mmol)

of EDCI · HCl, 0.153 g (1 mmol) of BtOH and 0.36 ml (4 mmol) of *N*-methylmorpholine in 70 ml of freshly distilled DMF, diluted with CH_2Cl_2 up to 1 l of total solvent volume. The reaction was allowed to proceed for 5 days at 3°; standard workup resulted in 460 mg (50%) and 370 mg (40%) of crude cyclopeptide, resp., which was pooled for prep. HPLC purification (*RP18* column; mobile phases A (H_2O/MeCN/CF_3COOH 970:30:1) and B (H_2O/MeCN/CF_3COOH 300:700:1), standard gradient system, flow rate 40 ml/min). Overall yield of ninhydrin-negative product was 520 mg after lyophilization, with correct amino-acid analysis and expected results in MS and ^{1}H-NMR. The cyclopeptide **1** was identical to material synthesized *via* azide cyclization from a linear precursor having N-terminal tyrosine and C-terminal proline (see above).

NMR Spectroscopy. All experiments were carried out in a magnetic field of 11.74 Tesla on a *Bruker-AMX-500* spectrometer. For all 2D experiments, the peptide concentration was 19 mg/ml in $CDCl_3$ or 11 mg/ml in DMSO. For the concentration studies in $CDCl_3$, the concentration was varied between 9 and 19 mg/ml. The temp. gradients of the amide protons were recorded in the range of 280–320 K for $CDCl_3$ and 300–340 K for DMSO. TOCSY Spectrum [8]: 16 scans, 512 points in t_1, 4096 points in t_2, relaxation delay 1.5 s, mixing length 80 ms. ROESY Spectrum: mixing scheme of short pulses [13c] with a field strength of 2 kHz with 48 scans, 512 points in t_1, 4096 points in t_2, relaxation delay 1.5 s, mixing length 136 ms. NOESY Spectrum [15]: identical spectral parameters, mixing time 150 ms. E.COSY Spectrum [14]: 16 scans, 512 points in t_1, 8192 points in t_2. HMQC Spectrum [9]: sweep widths 12.5 and 79.5 ppm in the ^{1}H and ^{13}C dimensions, resp.; 512 experiments of 1024 data points were collected with 48 scans, a relaxation delay of 200 ms, and an optimized delay after the BIRD scheme of 266 ms. HMQC-TOCSY Spectrum [10]: TOCSY mixing period 66 ms. HMBC Spectrum [11]: 216 scans, 512 points in t_1 of 8192 data points, relaxation delay 500 ms; sweep width in the ^{13}C dimension 92.5 ppm.

Computer Simulations. All simulations were carried out on *Silicon-Graphics-4D/240SX* and *-4D/70GT* work stations. The simulations using DMSO were previously described [20]. For the $CHCl_3$ simulations, the solvent was described as a four-point model using a united atom for the C- and H-atom. The solvent was considered rigid with the geometry (described by distances of 172 and 283 pm between CH and Cl and Cl and Cl, resp.) maintained by the application of SHAKE [24]. The charges and *Lennard-Jones* parameters were taken from the work of *Jorgensen* and coworkers [25].

An equilibrated box of DMSO (also treated as four points) [20] was used as a starting configuration for the $CHCl_3$, with the O-atom and two Me C-atoms of DMSO replaced by Cl-atoms. The correct geometry of the solvent was obtained by energy minimization. The box was then scaled to obtain the correct density of $CHCl_3$ and an MD simulation of 200 ps carried out to equilibrate the $CHCl_3$ soln. The final coordinate set from this simulation was used for the $CHCl_3$ simulations of hymenistatin 1 (**1**).

The MD simulations were carried out with the GROMOS program [26]. The peptide was placed in a periodic truncated octahedron of 20.3 nm^3 containing 143 $CHCl_3$ or 161 DMSO molecules. A step size of 2 fs employing SHAKE [24] was used with the nonbonded interactions updated every 25 steps with a cut-off distance of 1.2 nm. The simulations were run at 500 K with a tight coupling to a temp. bath [27] (a relaxation time of 20 fs) for an equilibration period of 20 ps. This temp. was reduced to 300 K, the coupling relaxed (200 fs), and the simulation continued for 100 ps.

The distance restraints were applied using standard procedures, a square potential well, using an error of ± 10% for the upper and lower distance restraints. Restraints for coupling constants were applied using a penalty function based on the difference between the experimental and calculated coupling constant [16]. This penalty function was shown to be quite effective in the generation of minimum-energy structures. The force constant was set to 2000 kJ mol^{-1} nm^{-2}, 1.0 kJ mol^{-1} Hz^{-2} and 0.25 kJ mol^{-1} Hz^{-2} for the NOE, ^3J(N*H*,*H*–C(α)) coupling constant and ^3J(*H*–C(α),*H*–C(β)) coupling constant restraints, resp.

After the restrained MD, the simulation was continued without the experimental constraints (free MD). The system was allowed to equilibrate (to the lack of restraints) for 20 ps and then the simulation continued for 200 ps. The atom-atom radial distribution functions were calculated following standard procedures [19].

Biological Testing. L1210 and P388 murine leukaemia cells were obtained from *G. Atassi* (*NCI* Brussels), KB human epidermoid carcinoma cells from *ATCC* (CCL 17), murine bone marrow cells were washed from femora of NMRI mice. Hymenistatin 1 (**1**) was dissolved in EtOH and diluted further with medium resulting in a final EtOH concentration in the assays of 0.5%.

Colony assays were performed by a method derived from that described by *Hamburger* and *Salmon* [28]. In short, an appropriate number of cells (L1210: 100; KB: 1000; bone marrow: 10000) were seeded in *Petri* dishes (⌀ 35 mm) in *RPMI-1640* medium with 10% fetal calf serum (FCS) (L1210) or 20% FCS (KB) or *Iscove's* medium with 20% horse serum and granulocyte-macrophage colony stimulating factor (GM-CSF) (murine bone marrow cells) in the presence or absence of **1**. The dishes were incubated at 37°, 95% rel. humidity, and 5% CO_2 (bone

marrow 10% CO_2) for 6 (L1210), 8 (KB), or 7 days (bone marrow). Then colonies consisting of more than 50 cells were counted using an automatic image analyzer, and the concentration resulting in the inhibition of colony formation by 90% was determined graphically.

Cytotoxicity assays with P388 cells were performed as described earlier [29]. In short, 15000 cells per well were seeded in *RPMI-1640* medium containing 20% FCS into the wells of microtiter plates and incubated for 24 or 48 h at 5% CO_2, 95% rel. humidity, and 37°. Then 10 µl of a soln. of 5 mg/ml MTT (= 3-(4,5-dimethylthiazol-2-yl)-2,5-diphenyl-2*H*-tetrazolium bromide) in phosphate-buffered saline were added and the plates incubated for further 30 min. Then color formation was measured in a microplate reader at 540 nm. Concentrations resulting in a 50% inhibition of color formation indicating a 50% reduction in cell number were determined graphically.

This work was finacially supported by *Fonds der Chemischen Industrie* and *Deutsche Forschungsgemeinschaft*. We thank Prof. *G. R. Pettit* for sending us the NMR spectrum of natural hymenistatin 1 (**1**) for comparison.

REFERENCES

[1] Y. Kato, N. Fusetani, S. Matsunaga, K. Hashimoto, *J. Am. Chem. Soc.* **1986,** *108,* 2780.
[2] M. Hagihara, S. L. Schreiber, *J. Am. Chem. Soc.* **1992,** *114,* 6570.
[3] J. Kobayashi, J. Cheng, M. R. Wälchli, H. Nakamura, Y. Hirata, T. Sasaki, Y. Ohizumi, *J. Org. Chem.* **1988,** *53,* 1800.
[4] C. Pathirana, P. R. Jensen, R. Swight, W. Fenical, *J. Org. Chem.* **1992,** *57,* 740.
[5] G. R. Pettit, P. J. Clewlow, C. Dufresne, D. L. Doubek, R. L. Cerny, K. Rützler, *Can. J. Chem.* **1990,** *68,* 708.
[6] R. B. Merrifield, *Angew. Chem.* **1985,** *97,* 801; *ibid. Int. Ed.* **1985,** *24,* 799.
[7] Y. S. Klausner, M. Bodanszky, *Synthesis* **1974,** 549.
[8] L. Braunschweiler, R. R. Ernst, *J. Magn. Reson.* **1983,** *53,* 521; A. Bax, D. G. Davis, *ibid.* **1985,** *65,* 355.
[9] A. Bax, S. Subramanian, *J. Magn. Reson.* **1986,** *67,* 565.
[10] A. Bax, L. Lerner, *J. Magn. Reson.* **1986,** *69,* 375.
[11] C. Griesinger, W. Bermel, K. Wagner, *J. Magn. Reson.* **1989,** *83,* 223; H. Kessler, P. Schmieder, M. Köck, M. Kurz, *ibid.* **1990,** *88,* 615.
[12] C. M. Deber, V. Madison, E. R. Blout, *Acc. Chem. Res.* **1976,** *9,* 106.
[13] a) A. A. Bothner-By, R. L. Stephens, J. Lee, C. D. Warren, R. W. Jeanloz, *J. Am. Chem. Soc.* **1983,** *106,* 811; b) A. Bax, D. G. Davis, *J. Magn. Reson.* **1985,** *63,* 207; c) H. Kessler, C. Griesinger, R. Kerssebaum, K. Wagner, R. R. Ernst, *J. Am. Chem. Soc.* **1987,** *109,* 607; d) C. Griesinger, R. R. Ernst, *J. Magn. Reson.* **1987,** *75,* 261.
[14] C. Griesinger, O. W. Sørensen, R. R. Ernst, *J. Magn. Reson.* **1987,** *75,* 474.
[15] J. Jeener, B. H. Meier, P. Bachmann, R. R. Ernst, *J. Chem. Phys.* **1979,** *71,* 4546; R. Baumann, G. Wider, R. R. Ernst, K. Wüthrich, *J. Magn. Reson.* **1981,** *44,* 402; S. Macura, Y. Huang, O. Suter, R. R. Ernst, *ibid.* **1981,** *43,* 259.
[16] a) Y. Kim, J. H. Prestegard, *Proteins Struct. Funct. Genet.* **1990,** *8,* 377; b) D. F. Mierke, H. Kessler, *Biopolymers* **1992,** *32,* 1277.
[17] a) G. Rose, L. M. Gierasch, J. A. Smith, *Adv. Protein Chem.* **1985,** *37,* 1; b) G. Müller, M. Gurrath, M. Kurz, H. Kessler, *Proteins Struct. Funct. Genet.* **1993,** *15,* 235.
[18] J. Saulitis, D. F. Mierke, G. Byk, C. Gilon, H. Kessler, *J. Am. Chem. Soc.* **1992,** *114,* 4818.
[19] M. P. Allen, D. J. Tildsely, 'Computer Simulation of Liquids', Clarendon Press, Oxford, 1987.
[20] D. F. Mierke, H. Kessler, *J. Am. Chem. Soc.* **1991,** *113,* 9466.
[21] P. M. Dean, 'Molecular Foundations of Drug-Receptor Interaction', Cambridge University Press, Cambridge, 1987.
[22] E. Kaiser, R. L. Colescot, C. D. Bossinger, P. I. Cook, *Anal. Biochem.* **1970,** *34,* 595.
[23] E. Kaiser, C. D. Bossinger, R. L. Colescot, D. B. Olsen, *Anal. Chim. Acta* **1980,** *118,* 149.
[24] J. P. Ryckaert, G. Ciccotti, H. J. C. Berendsen, *J. Comput. Phys.* **1977,** *23,* 327.
[25] W. Jorgensen, J. M. Briggs, M. L. Contreras, *J. Phys. Chem.* **1990,** *94,* 1683.
[26] W. F. van Gunsteren, H. J. C. Berendsen, 'Groningen Molecular Simulation Library Manual (GROMOS)', Biomos B.V., Groningen, 1987.
[27] H. J. C. Berendsen, J. P. M. Postma, W. F. van Gunsteren, A. DiNola, J. R. Haak, *J. Chem. Phys.* **1984,** *81,* 3684.
[28] A. W. Hamburger, S. E. Salomon, *J. Clin. Invest.* **1977,** *60,* 846.
[29] M. Iselt, W. Holtei, P. Hilgard, *Arzneim.-Forsch./Drug Res.* **1989,** *39,* 747.